Biochimie 111 (2015) 58–69

Contents lists available at ScienceDirect

Biochimie

journal homepage: www.elsevier.com/locate/biochi

Research paper

# Crystal structure analysis of peroxidase from the palm tree *Chamaerops excelsa*

Amanda Bernardes [a, 1], Larissa C. Textor [a, 1], Jademilson C. Santos [a, 1], Nazaret Hidalgo Cuadrado [b, 2], Eduard Ya. Kostetsky [c], Manuel G. Roig [b], Vassiliy N. Bavro [e], João R.C. Muniz [a], Valery L. Shnyrov [d], Igor Polikarpov [a, *]

[a] Instituto de Física de São Carlos, Universidade de São Paulo, Av. Trabalhador Sãocarlense 400, São Carlos, SP 13560-970, Brazil
[b] Departamento de Química Física, Facultad de Química, Universidad de Salamanca, 37008 Salamanca, Spain
[c] Departament of Biochemistry, Microbiology and Biotechnology, Far Eastern Federal University, 690600 Vladivostok, Russia
[d] Departamento de Bioquímica y Biología Molecular, Facultad de Biología, Universidad de Salamanca, 37007 Salamanca, Spain
[e] Institute of Microbiology and Infection, University of Birmingham, Birmingham B152TT, United Kingdom

ARTICLE INFO

*Article history:*
Received 29 July 2014
Accepted 25 January 2015
Available online 7 February 2015

*Keywords:*
Plant peroxidase
*Chamaerops excelsa*
Oxidoreductases
Protein crystallography
Protein oligomerization

ABSTRACT

Palm tree peroxidases are known to be very stable enzymes and the peroxidase from the *Chamaerops excelsa* (CEP), which has a high pH and thermal stability, is no exception. To date, the structural and molecular events underscoring such biochemical behavior have not been explored in depth. In order to identify the structural characteristics accounting for the high stability of palm tree peroxidases, we solved and refined the X-ray structure of native CEP at a resolution of 2.6 Å. The CEP structure has an overall fold typical of plant peroxidases and confirmed the conservation of characteristic structural elements such as the heme group and calcium ions. At the same time the structure revealed important modifications in the amino acid residues in the vicinity of the exposed heme edge region, involved in substrate binding, that could account for the morphological variations among palm tree peroxidases through the disruption of molecular interactions at the second binding site. These modifications could alleviate the inhibition of enzymatic activity caused by molecular interactions at the latter binding site. Comparing the CEP crystallographic model described here with other publicly available peroxidase structures allowed the identification of a noncovalent homodimer assembly held together by a number of ionic and hydrophobic interactions. We demonstrate, that this dimeric arrangement results in a more stable protein quaternary structure through stabilization of the regions that are highly dynamic in other peroxidases. In addition, we resolved five N-glycosylation sites, which might also contribute to enzyme stability and resistance against proteolytic cleavage.



## 1. Introduction

Peroxidases (EC 1.11.1.7; donor: hydrogen peroxide oxidoreductase) are heme proteins that catalyze the oxidoreduction of a broad variety of peroxides. Most commonly, peroxidases catalyze the oxidation of organic substrates, while reducing $H_2O_2$ to water. This process involves multiple-reactions and a number of intermediate enzyme forms, and is known as the Poulos–Kraut mechanism, which plays a key role in several metabolic responses of all peroxidases [1]. Peroxidases are important for many biological responses and processes, such as defense against pathogenic microorganisms, cell wall formation, and lignification [2].

The peroxidase superfamily includes animal and non-animal peroxidases, and the latter are generally subdivided into three classes, all sharing a similar three-dimensional fold despite their low amino acid sequence identity [3,4]. Class I includes intracellular enzymes, such as plant ascorbate peroxidases, yeast cytochrome c peroxidases and bacterial catalases. Class II is composed of secreted peroxidases encoded exclusively by fungal organisms, including lignin peroxidase and $Mn^{2+}$-dependent peroxidases. Finally, Class III consists of secreted plant peroxidases with molecular weights

* Corresponding author.
*E-mail address:* ipolikarpov@ifsc.usp.br (I. Polikarpov).
[1] These authors contributed equally to the work.
[2] Present address: Instituto de Estudios Biofuncionales, Departamento de Química-Física II, Facultad de Farmacia, Universidad Complutense de Madrid, 28040 Madrid, Spain.

http://dx.doi.org/10.1016/j.biochi.2015.01.014
0300-9084/

between 28 and 60 kDa [3,5]. The Class III plant peroxidases perform a number of functions, *e.g.*: lignin and suberin formation, the cross-linking of cell wall components, and the synthesis of phytoalexins [6].

It is generally accepted that only Class I enzymes are able to form multimers (dimers and tetramers) while the enzymes of other classes are monomeric and glycosylated. At the same time, multimerization is a very common feature of many mammalian peroxidases that exert their functions as dimers [7,8]. Despite the physiological importance of this phenomenon, little information is available about the multimerization of plant peroxidases. A dimeric structure for recombinant horseradish peroxidase has been reported previously in micellar systems [7] and water solutions [9], but it has not been observed for the native enzyme. Dimerization affects enzyme stability, activity and the immobilization of physical surfaces [9]. The absence of dimeric quaternary structures of native peroxidase was explained in terms of the high degree of its glycosylation. Heavy glycosylation and enzyme dimerization were also proposed to be the molecular events accounting for the greater stability of palm tree peroxidases [10,11]. Once the peroxidases from the leaves of tropical plants, such as palm trees, were shown to have high stability, it became crucial to study the quaternary structure of these enzymes. The high stability of the palm tree peroxidases makes them ideal for biotechnological applications and of direct interest to the industry. That is why it became crucial to establish their structure as it impacts immobilization. However, the increased stability of proteins is frequently not a consequence of a single mechanism but instead involves a combination of several factors, including disulfide bond formation, multimerization and glycosylation [10,12].

Structurally, peroxidases are mainly composed of α-helices and can be divided into two domains: one containing the heme group, and the other with a ferriprotoporphyrin prosthetic group, both located inside of a hydrophobic pocket [13].

Class I peroxidases are not glycosylated, whereas the second and third classes are glycosylated peroxidases with 2–8 N-linked glycans known to contribute to the protein stabilization [14]. Similarly, Class I peroxidases do not contain any disulphide bonds or calcium ions. However, all cysteine residues present in Class II and III enzymes form disulfide bonds, conferring those enzymes higher rigidity. Class II peroxidases also show two calcium-binding sites that have important structural and functional roles. Despite the differences between the peroxidase subfamilies, their similar 3D fold is preserved [13].

To date, several peroxidases from tropical palm-trees – *Elaies guineensis*, *Roystonea regia*, *Trachycarpus fortunei* and *Chamaerops excelsa* (*T. fortunei*) – have been isolated and characterized [15–18]. These are structurally and functionally stable enzymes that exhibit higher thermal stability within a broad pH range and in the presence of denaturing agents in comparison to the well-studied horseradish peroxidase (HRP), soybean seed-coat peroxidase (SBP) and anionic peanut (*Arachis hypogaea* L.) peroxidase. It has been demonstrated that CEP is a highly stable enzyme over a pH-range of 2.5–10.0, with no noteworthy changes in enzymatic activity [19,20]. Since enzymes that tolerate extreme pH and temperature conditions are important for various biotechnological applications, the commercial use of such peroxidases is of major interest, especially in the biocatalysis industry. Indeed, assays using modified electrodes of adsorbed anionic royal palm tree peroxidase (RPTP), anionic sweet potato peroxidase (SPP) and cationic horseradish peroxidase (HRP-C) as biosensors for the detection of hydrogen peroxide revealed that the RPTP-based electrodes are more sensitive and exhibit a wider linear range and a higher storage stability [21]. Accordingly, the unique catalytic and stability profile of these palm peroxidases is testimony to their potential as biocatalysts and biosensors for other biotechnological applications [22–24].

Although the three-dimensional structures of a considerable number of peroxidases have been determined, to date only a few of those belong to Class III plant peroxidases: horseradish [25], peanut [26], barley [27], thale cress [28], soybean [29] and royal palm tree [15]. Despite this, the exact structural features responsible for the improved properties of the palm tree peroxidases as compared to other plant peroxidases remain obscure.

In the present work, we solved the three-dimensional X-ray crystallographic structure of a Class III plant peroxidase isolated from the leaves of the palm tree *C. excelsa* (CEP) and compared it to other available peroxidase structures. Additionally, the new quaternary structure identified for CEP and for royal palm tree peroxidase (RPTP) [15] offers possible explanations for their high thermal stability. Our results provide new insights into the structure–function relationships of plant peroxidases and their quaternary structures.

## 2. Materials and methods

### 2.1. Enzyme purification

CEP was purified from the palm tree *C. excelsa* as described previously [30]. Briefly, leaves (1820 g) from a three-year-old palm tree were milled and homogenized in 7.28 l distilled water for 22–24 h at room temperature. Excess material was removed by vacuum filtration and centrifugation (10, 000 g, 277 K for 15 min). Pigments were extracted by phase separation over approximately 20 h at 277 K after the addition to the supernatant of solid PEG at 14% (w/v) and solid ammonium sulfate at 10% (w/v). Two phases were formed after the addition of ammonium sulfate: an upper polymer phase (dark brown in color) containing pigments, phenols, polyphenols, oxidized phenols and PEG, and a lower aqueous phase (yellow in color) containing peroxidase. Each phase consisted of 50% of the initial volume. These phases were separated and the phase containing peroxidase activity was centrifuged. The clear supernatant containing peroxidase activity was titrated with ammonium sulfate to a conductivity value of 232 mS $cm^{-1}$ and applied on a phenyl-Sepharose column (1.5 × 35 cm) equilibrated with 100 mM phosphate buffer, pH 6.5, with 1.7 M ammonium sulfate, with the same conductivity as the sample. The enzyme was eluted with 100 mM phosphate buffer, pH 6.5, plus 0.2 M ammonium sulfate at a flow rate of 1 ml $min^{-1}$. 15-ml fractions were collected and those showing peroxidase activity were dialyzed against 5 mM Tris buffer, pH 9.3, for 72 h with constant stirring at 277 K. These fractions were membrane-concentrated (Amicon, 10 kDa cutoff) to 15 ml and applied on a TSK-Gel DEAE-5PW column (1 × 30 cm) equilibrated with 5 mM Tris buffer, pH 9.3. Elution was carried out with a linear 0–300 mM NaCl gradient in the same buffer at a flow rate of 1 ml $min^{-1}$. The fractions with peroxidase activity were collected, membrane-concentrated (Amicon, 10 kDa cutoff) and applied on a Superdex-200 column equilibrated with 5 mM Tris buffer, pH 9.3. Elution was carried out in the same buffer at a flow rate of 1 ml $min^{-1}$. Finally, the peroxidase was dialyzed against distilled water and freeze-dried.

Protein purity and quality were analyzed by native and denaturing polyacrylamide gel electrophoresis (PAGE), using gel concentrations in a gradient of 8%–25% and 15% SDS, respectively, as well as by UV–visible spectrophotometry (RZ = $A_{403}/A_{280}$ = 2.8–3.0). Analysis of the oligomeric state and polydispersity of the enzyme at three different concentrations was carried out by dynamic light scattering (DLS), using the Zetasizer μV (Malvern Instruments Ltd.). Measurements of as minimum of 13 data points

at 293 K were taken in triplicate from enzyme solutions of 2.5, 5 and 10 mg $ml^{-1}$.

### 2.2. Crystallization and data collection

The lyophilized purified peroxidase, isolated from *C. excelsa* palm tree, was re-suspended in 50 mM Tris buffer at pH 8.0 to a final concentration of 10 mg $ml^{-1}$. Crystals were obtained using the hanging-drop vapor diffusion technique in 0.17 M ammonium sulfate, 0.085 M Tris, pH 8.0, 17% PEG MME 2000 and 15% glycerol, as previously described [30]. The diffraction data were collected at the MX2 beamline [31] of the Brazilian National Synchrotron Laboratory (LNLS, Campinas, Brazil) using a Marmosaic225 detector and monochromatic synchrotron radiation with a wavelength of 1.4586 Å. The data, which extended to a resolution of 2.6 Å, were integrated and scaled with the XDS program [32]. The crystals belonged to the $P2_12_12_1$ space group, with unit cell parameters of $a = 70.2$ Å, $b = 100.7$ Å, $c = 132.3$ Å [30].

### 2.3. Molecular replacement, model building and structure refinement

The crystallographic structure was determined by molecular replacement (MR) with the Phaser program [33], using the atomic coordinates of the royal palm tree *R. regia* peroxidase (RPTP, PDB id 3HDL) [15] as template. With 87% of sequence identity, the search model was manipulated prior to MR rotation and translation functions in order to remove non-bonded atoms, covalently attached carbohydrates, and the heme group.

The $2F_o - F_c$ electron density map calculated from the unique solution of the top rotation and translation searches revealed a clear and contiguous electron density for the protein and active site molecules not included in the search model. Model building and refinement was carried out using Coot [34]. Cycles of restrained refinement with the Refmac5 [35] were initially carried out using overall temperature factors and later with isotropic atomic temperature factors. Water molecules were added using Arp/wArp [36] and the stereochemical quality of the model was validated with the MolProbity program [37]. The statistics of the refined structures are given in Table 1. The visualization and all representations of the structures were carried out using PyMol (The PyMOL Molecular Graphics System, Version 1.2r3pre, Schrödinger, LLC).

**Table 1**
Data collection and refinement statistics. Values in parenthesis refer to the outer shell.

| Data collection | Peroxidase |
|---|---|
| Wavelength/beamline | 1.4586/MX2, LNLS |
| Space group | $P2_12_12_1$ |
| Unit cell dimensions (Å) | 70.18; 100.65; 132.31 |
| Resolution (Å) | 80.11–2.60 (2.69–2.60) |
| Number of unique reflections | 29,525 (5779) |
| Mosaicity (°) | 0.5 |
| Multiplicity | 4.3 (4.3) |
| Completeness (%) | 90.1 (91.8) |
| $R_{merge}$ [a] (%) | 10.1 (55.3) |
| Wilson B-factor ($Å^2$) | 43.82 |
| Mean I/σ(I) | 10.54 (3.83) |
| *Refinement* | |
| $R_{work}/R_{free}$ [b] (%) | 21.8/24.6 |
| R.m.s. deviations | |
| Bond lengths (Å) | 0.021 |
| Bond angles (°) | 1.760 |
| Ramachandran outliers (%) | 0 |
| PDB ID | 4USC |

[a] $R_{merge} = \sum hkl \sum i |Ii(hkl) - \langle I(hkl)\rangle| / \sum hkl \sum i |Ii(hkl)|$, where $\langle I(hkl)\rangle$ is the mean $I(hkl)$ over symmetry-equivalent reflections.

[b] $R_{factor}/R_{free} = \sum hkl |F_{obs} - F_{calc}| / \sum hkl |F_{obs}|$, where $F_{obs}$ and $F_{calc}$ are the observed and calculated structure factors respectively. $R_{free}$ was calculated using 5% of the total reflections, which were chosen randomly and omitted from the refinement.

## 3. Results and discussion

### 3.1. Structure determination

Crystal plates grew after approximately 24 h and reached their maximum size after one week [30]. Despite having a rather thin plate-shaped morphology, these crystals were found to be suitable for X-ray data collection. The crystals of native CEP belonged to the $P2_12_12_1$ space group, had a solvent content of 42% and diffracted to 2.6 Å resolution. The final $R_{factor}$ and $R_{free}$ for the refined structure were 21.8 and 24.6% respectively. The quality of the final model was checked using the MolProbity server [37]. Crystallographic parameters are summarized in Table 1.

### 3.2. Overall three-dimensional structure

The final model shows two molecules of the enzyme per asymmetric unit, assembled in a homodimer consisting of 303 residues per monomer, giving total molecular weight of 50 kDa. Each monomer contained one heme prosthetic group and two calcium ions, which were presumably co-purified together with the native protein. The heme group, bound non-covalently to an inner binding cavity of peroxidase, has a clear electron density and is surrounded by highly conserved amino acid residues, essential for maintaining it properly aligned and functional [38]. Each protein chain has 7 clearly defined N-glycosylation sites. Furthermore, molecules of glycerol, sulfate and polyethylene glycol were also modeled in the asymmetric unit cell.

The overall fold CEP is typical of the Class III peroxidase family [15,25,26,29]. It comprises 15 α-helices that form a structural scaffold (Fig. 1A), with two small helices inserted between the B and C helices. Similar to other Class III peroxidases, CEP also contains two short anti-parallel β-strands. The structure is split into two distinct domains, distal and proximal, each of which contains a calcium-binding site. $Ca^{2+}$ ion is coordinated through an extensive hydrogen-bonding network. The following residues were found to form this network: D43, D46, D48, D50, S52, E64 and one water molecule (w2) in the distal domain, and S170, D223, T226, V229 and D231 in the proximal domain (Fig. 1B) respectively. The presence of these ions is an important feature of peroxidase structures since they are responsible for the formation of a functional active site conformation and their loss severely impacts enzyme activity [39–41]. The heme group is inserted between the distal and proximal domains, between the B and F helices.

Four disulfide bonds (Cys11-Cys91, Cys44-Cys49, Cys97-Cys299 and Cys176-Cys208) are highly conserved among all members of Class III peroxidases and ensure the stabilization and integrity of the enzyme's structure. In particular, the Cys176-Cys208 disulfide bond stabilizes a long insertion between the F and G helices, which is a characteristic feature of Class III peroxidases [25].

The chains of the two molecules in the asymmetric unit overlay very closely with a Root Mean Square Deviation (RMSD) of 0.142 Å (over 282 residues, considering C-alphas only). The positions of the heme groups and calcium ions are conserved. The importance of the conservation of these structural elements for the structure and function of peroxidases, and their critical role in the thermal and chemical stabilities of these enzymes have been highlighted previously [42,43].

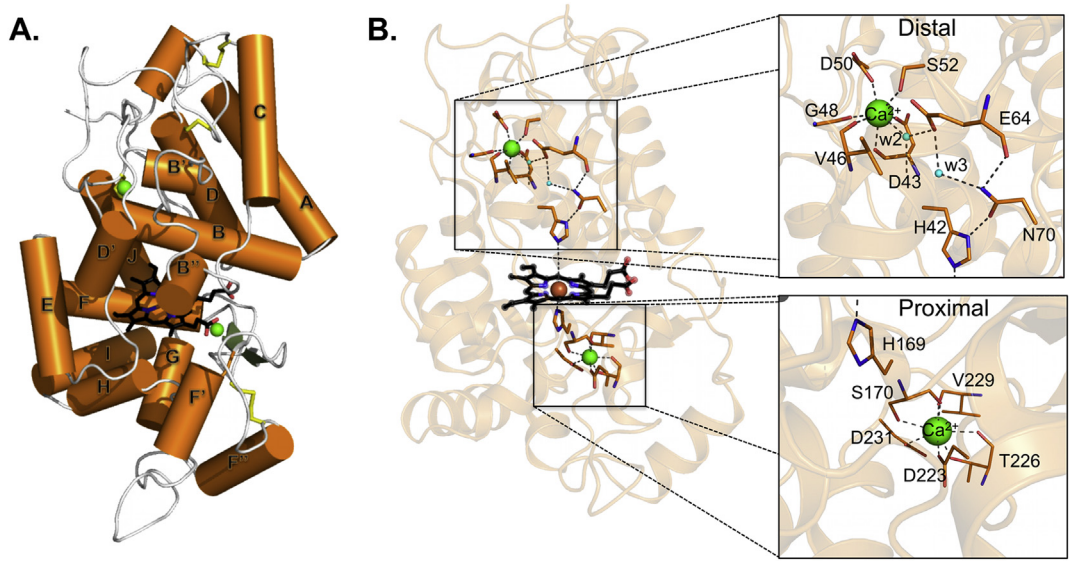


**Fig. 1.** Three-dimensional representation of the X-ray crystal structure of CEP. A. A schematic diagram of CEP, with the helices shown in orange and labeled according to Patterson and Poulos (1995). There are also four sulfide bonds, displayed in stick and yellow, those ensure protein structure stabilization. The heme group (black stick) is located between the distal and proximal domains. B. Close-up views of distal and proximal calcium-binding sites, where the seven bonds that generate the coordination of the ions (green spheres) are represented with dashed black lines, and the residues responsible for this with sticks.

### 3.3. Molecular mechanisms of the peroxidase activity

Peroxidases participate in broad range of reactions occurring in the living processes, such as the protection of tissues from pathogenic microorganisms, suberization, auxin catabolism, defense, stress etc. [44]. However, in chemical terms peroxidases convert toxic $H_2O_2$ into water molecules. The molecular catalysis mechanism commences with the binding of $H_2O_2$ to the high-spin ferric heme ion of he resting peroxidase, followed by heterolytic cleavage of the peroxide oxygen–oxygen bond under the influence of highly conserved histidine and arginine residues in the active site [45–47]. The methodological analysis of the kinetic mechanism of the $H_2O_2$-assisted CEP-catalyzed oxidation of reducing substrates was investigated using initial rate measurements, in which the concentrations of both the $H_2O_2$ and the substrate were varied systematically, and the results were analyzed assuming steady-state conditions. This investigation demonstrates that these enzymes act according to a ping-pong Bi–Bi reaction mechanism of substrate inhibition, following the Michaelis–Menten saturation kinetic model. This mechanism was found to be similar in both palm tree enzymes, CEP and RPTP [48].

In the absence of substrate, or when the enzymes are exposed to high concentration of hydrogen peroxide, this latter can act as a suicide substrate of peroxidases that converts Compound II into a highly reactive peroxy-iron(III) porphyrin-free radical named Compound III [49]. This mechanism is known as suicide inactivation of peroxidases by $H_2O_2$ [50] and for several peroxidases, including CEP, the kinetics of suicide inactivation by $H_2O_2$ is time dependent with saturation [38].

A dimeric quaternary structure is thought to be essential for a fully functional active site, since the active site is formed by amino acid residues from both subunits. The dimeric structure has also been shown to be involved in the stabilization of the tertiary structures of individual subunits as well as to provide a non-substrate ligand-binding site at the dimer interface [51]. These results indicate that the peculiarities of the CEP active site are involved not only in the improvement of catalytic efficiency but also in the prevention of $H_2O_2$ inactivation. In sum, CEP is the most active of all peroxidases known at present and a very robust enzyme that exhibits extraordinary resilience against inactivation by $H_2O_2$. These observations prompted us to perform a detailed structural analysis of CEP and its dimerization.

#### 3.3.1. Structural alignment of CEP with homologous peroxidases

In order to identify possible differences between several Class III plant peroxidases that may be responsible for their unique properties, we initially performed an amino acid sequence alignment with structurally characterized homologous peroxidases from other organisms (Fig. 2), including *R. regia* (royal palm tree (RPTP), PDB id: 3HDL [15]), *Arabidopsis thaliana* (thale cress (ATP A2), PDB id: 1PA2 [28]), *Raphanus sativus* (radish (RSP), PDB id: 4A5G), *Glycine max* (soybean (SBP), PDB id: 1FHF [29]), *Armoracia rusticana* (horseradish (HRP-C), PDB id: 1ATJ [25]), *Arachis hypogala* (peanut (PNP), PDB id: 1SCH [26]) and *Hordeum vulgare* (barley (BP1), PDB id: 1BGP [27]).

The sequence alignment confirmed the high level of conservation between the CEP and RPTP palm peroxidases (86% of sequence identity) and a medium level of identity with other Class III plant peroxidase sequences (sequence identity around 40%).

Overall, the more significant variations in the amino acid identity were concentrated in the vicinity of the peptide segment between the F and H helices, comprising the inserted F′ and F″ helices. These additional helices are one of the main characteristics that distinguish Class III peroxidases and this region has been described as being responsible for substrate recognition and binding [13,15,52,53]. Even for the two palm tree peroxidases, which have a high level of amino acid sequence identity, the region between the F and H helices appears more variable in comparison to the rest of the structure (Fig. 2 – red square).

The positions of the secondary structural elements are conserved (Fig. 3) with RMSDs of about 1 Å, considering the Cα position of each structure. The most variable regions observed in the 3D structures of the enzyme encompass the auxiliary helixes and loops between the F and H helices as well as the loop between residues Ser57 and Ala63 (Fig. 3).

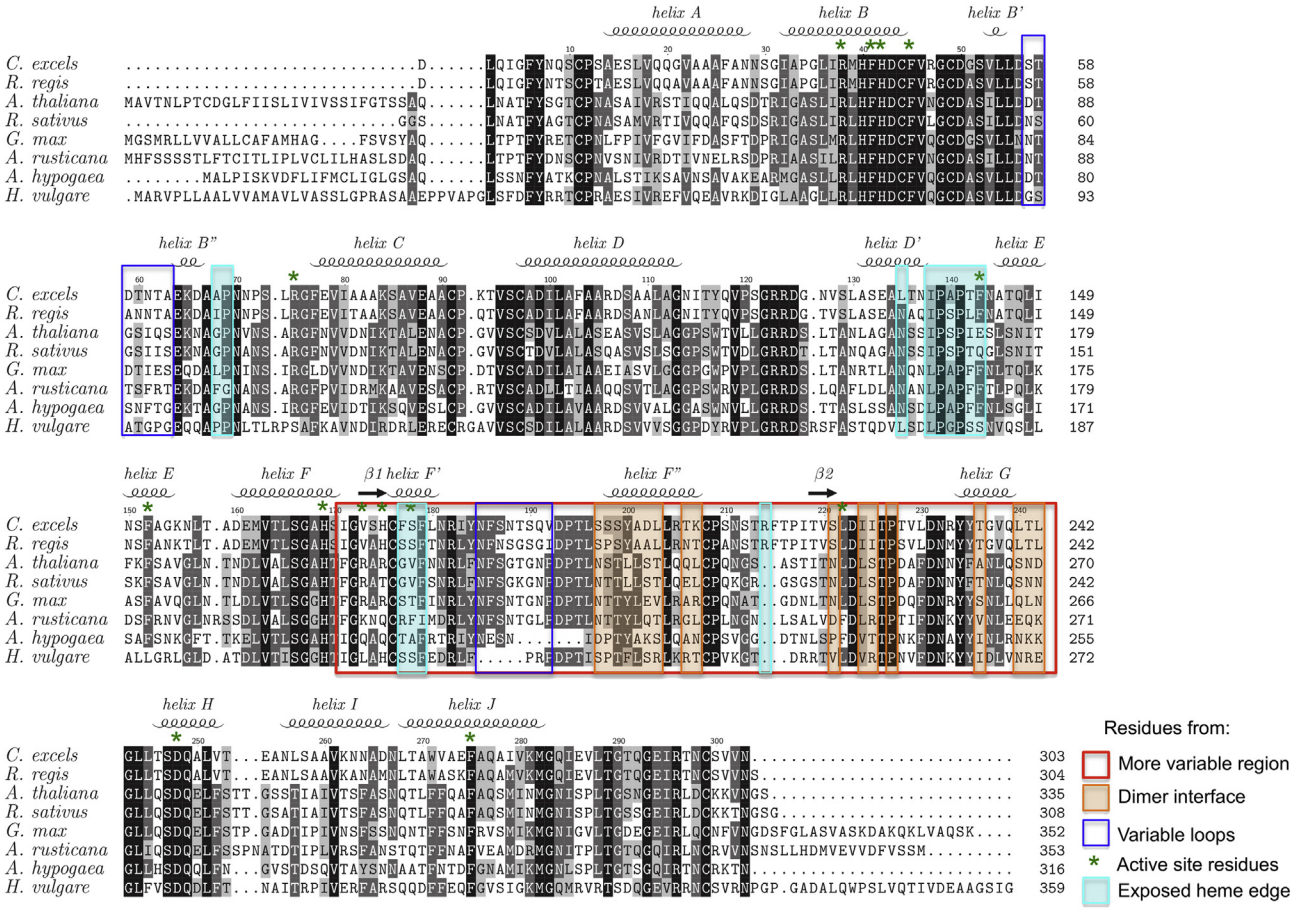


**Fig. 2.** Multiple alignments of amino acid sequences of Class III peroxidases. Relevant residues are indicated with different colors.

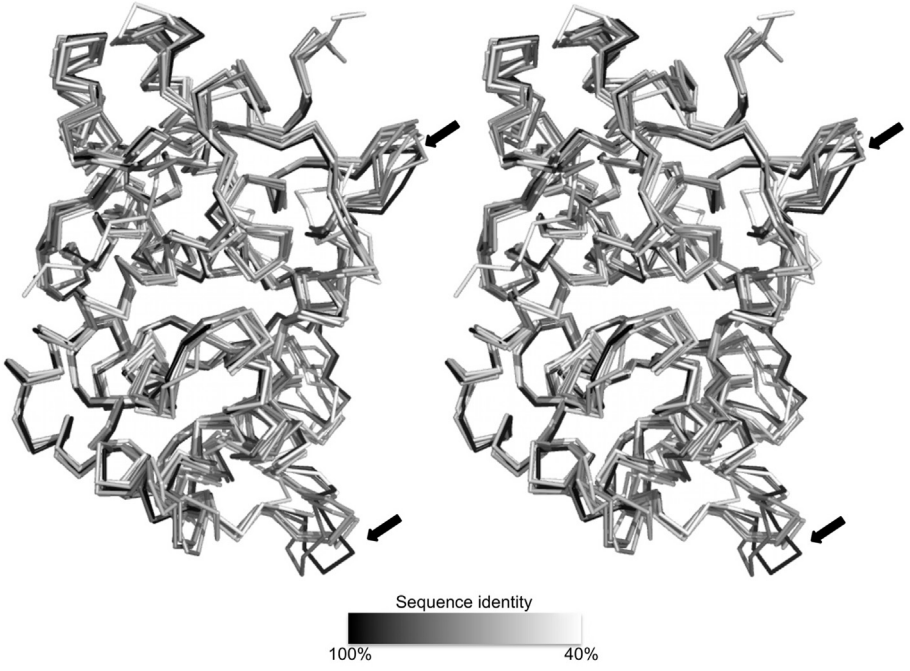


**Fig. 3.** Stereo view of the three-dimensional structure of several Class III peroxidases. Superimposed Cα trace of CEP and high-sequence identity peroxidases. The "Loop 1" and "Loop 2" indicated are the most variable loops found in the structures and they are composed of residues Ser57-Ala63 and Asn185-Val192, respectively.

*3.3.2. Enzyme active site*

The active site and heme pocket of CEP resembles that observed in other plant peroxidases, with the iron atom in the central heme plane. The structure of CEP has been solved with the heme group in a balance between its resting state and the hydroperoxide complex state, which is manifested as a refined occupancy of peroxide bound to a heme group equal to 30%.

Correct orientation of the heme group is critical for peroxidase catalysis and is provided through interactions with surrounding residues. In the structure of CEP, the residues involved in heme-group stabilization are Arg38, Arg75, Val173, His175 and Ser178 (Fig. 4). All of these residues, except R38, form hydrogen bonds directly with the side chain of heme propionates, whereas a water molecule mediates the interaction of Arg38 with the latter moiety. According to the Poulos–Kraut mechanism for peroxide catalysis [45], the Arg38 and His42 residues are key molecular components in the heterolytic cleavage of the peroxide O–O bond. Arg38 aids in the charge stabilization of the peroxidase:$H_2O_2$ complex, and His42 acts as a transitory proton acceptor [15]. Another important interaction is that occurring between the iron atom of the heme group and His169, which promotes the coordination of this metal atom. This residue is also involved in a hydrogen bond formation with Asp248, responsible for endowing the proximal histidine ligand with a more imidazole-like character [26,54].

In addition to polar interactions, several hydrophobic interactions are also involved in the maintenance of the prosthetic group, which including the residues Phe41, Phe45, Phe143, Phe152 and Phe275 (Fig. 4). The first phenylalanine cited (Phe41) has already been described to have functions related to the peroxigenase activity of enzymes because of the p-stacking interaction with the heme porphyrin ring promotes a restricted access of the iron atom [15,55].

Superposition of the amino acid residues in the close vicinity of the heme groups at the active sites of CEP and RPTP shows that they are virtually identical (Fig. 4), thus failing to provide structural insight into the observed differences in their catalytic activity. Accordingly we analyzed the channel that provides access to the heme pocket in more detail.

*3.3.3. Substrate access channel – exposed heme edge*

It is well known that substrates interact with peroxidases through the exposed heme edge, which includes the channel that connects the molecular surface and the distal heme pocket. For this reason, it is accepted that the residues of this region modulate the substrate specificities of peroxidases (Fig. 5A) [13,52,53,56,57].

There is a significant sequence divergence in the amino acid residues that line-up the substrate access channel, thus introducing differences in both the specificity and activity of peroxidases [38]. For the CEP structure, the channel is aligned by the following residues: Ala68, Pro69, Leu135, Ile138, Pro139, Ala140, Pro141, Thr142, Phe143, Phe177, Ser178, Phe179 and Arg214, (Fig. 2 – residues highlighted in cyan), located mainly at the loop between the D′ and E helices and at the F′ helix. All the prolines are highly conserved in all the plant peroxidase sequences analyzed, but the identity of other residues shows considerable variations. Residues Ala68, Ala140, Thr142 and Phe177 of the CEP molecule are substituted, respectively, by Ile68, Ser140, Leu142 and Ser177 in the RPTP structure (Fig. 5B). The most significant modifications are induced by the Ala68 to Ile68 and Phe177 to Ser177 substitutions. The first modification is located at the upper side of the channel entry, which broadens into the CEP binding channel as a result of the smaller side chain of the Ala68 residue present as compared to that of Ile68 of RPTP (Fig. 5C). By contrast, the Phe177 to Ser177 substitution is located at the opposite margin of the tunnel, thus decreasing the opening of the CEP channel at this location (Fig. 5D). Accordingly, the morphology of the channel, which guarantees access of the substrates to the heme group, is very different between CEP and RPTP and this seems to have a strong influence on the specificity and activity of the enzymes.

It is also noteworthy that the Ala140 residue in CEP is replaced by a serine residue (Ser140) in the RPTP molecule. In the latter structure, the Ser140 side-chain hydroxyl group forms a water-mediated hydrogen bond with the oxygen atom of the MES buffer molecule, which is additionally bound to RPTP by a long-range interaction between its sulfuric oxygen atom and the Arg214 residue. In the structure of RPTP, the MES molecule is positioned close to a potential secondary substrate-binding site, as has also been reported in SBP:TRIS and HRP-C:ferulic acid complexes [29,58]. The presence of buffer molecules bound to peroxidases suggests that these substances could be potential inhibitors of peroxidase enzymatic activity [15]. No buffer molecules are observed in the same region of the CEP structure. One possible explanation is that the serine to alanine substitution at position 140 eliminates the potential hydrogen bond with the buffer molecule. Furthermore, the Ser177 of RPTP is replaced by a phenylalanine in the CEP structure. The bulkier side chain of phenylalanine would cause steric hindrance with the MES molecule. Therefore, both the loss of the

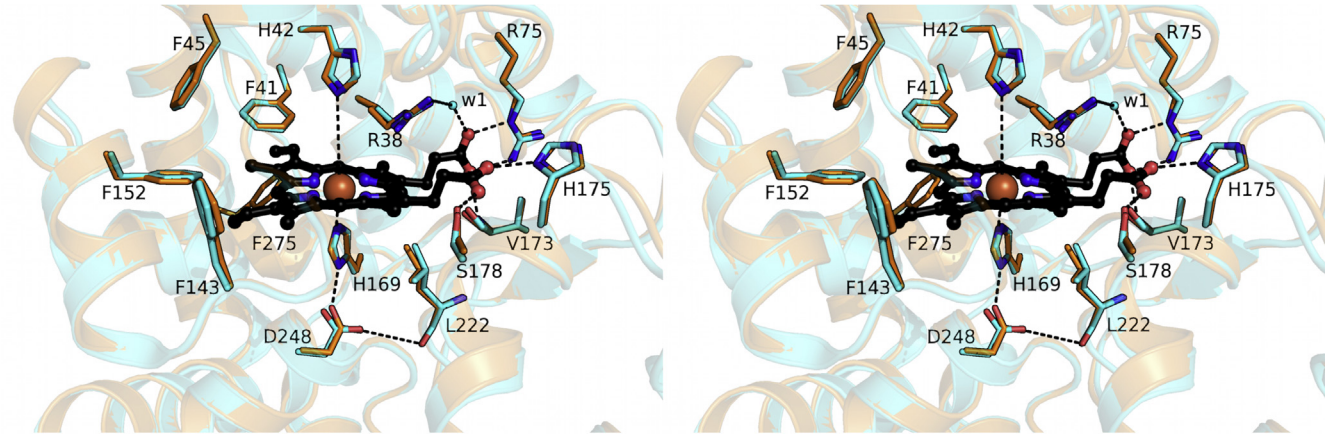


**Fig. 4.** Stereo view of structural features of the CEP active site and superposition with the RPTP active site. Surrounding the heme prosthetic group (ball, stick and black) there are key catalytic residues shown in stick representation. Heme environment of CEP and RPTP, exhibiting several conserved aromatic residues that form a hydrophobic cluster. The interactions between the heme propionyl and protein backbone are indicated as dashed black lines. CEP is represented in orange and RPTP in cyan.

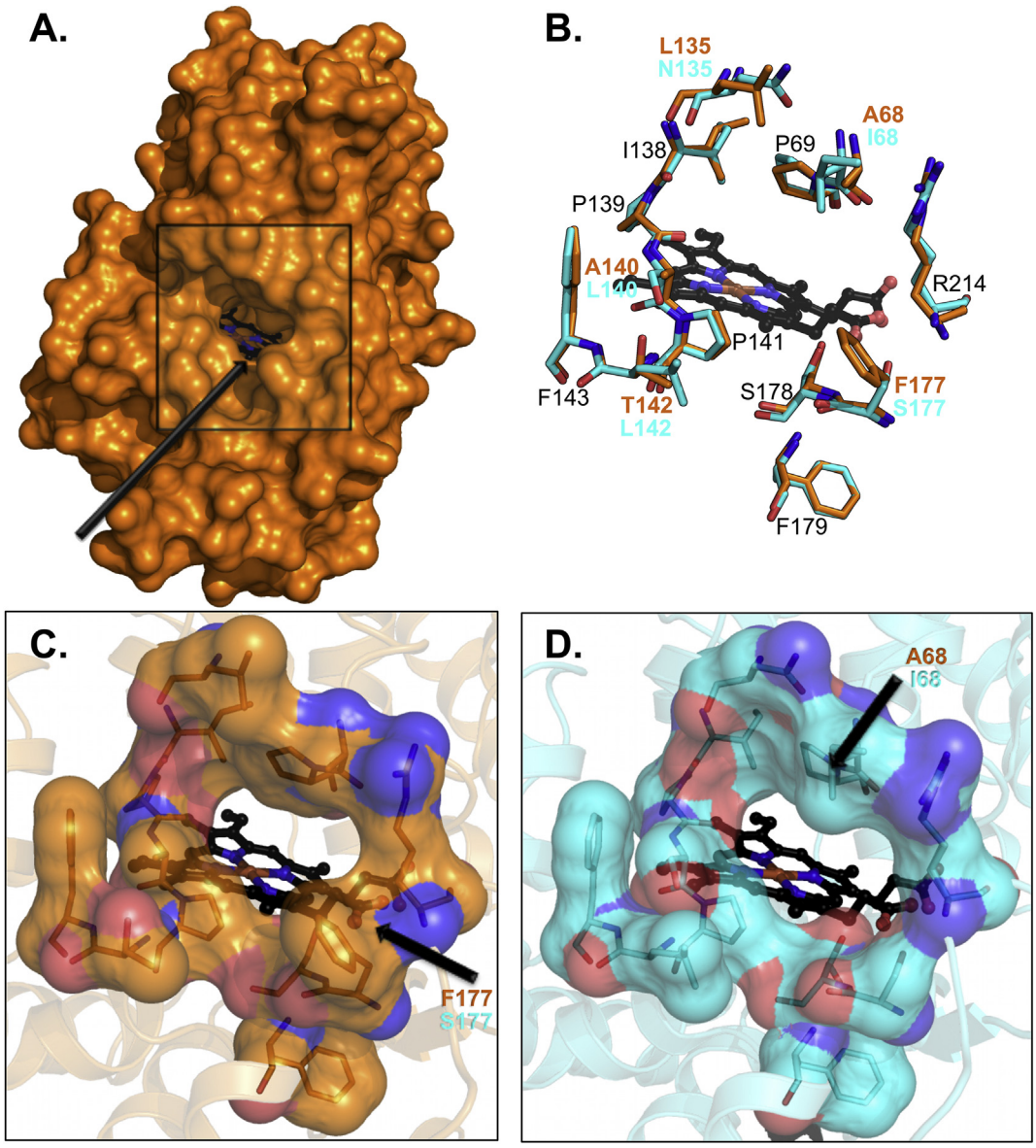


**Fig. 5.** Channel that connects the molecular surface and the distal heme pocket. A. Surface representation of the CEP structure, with a black arrow specifying the substrate access channel and the exposed heme edge. B. Stereo representation of superimposed residues of heme exposure of CEP (orange) and RPTP. All replaced residues are shown with the respective color of each protein. Comparative views of the distal heme exposure of C. CEP and D. RPTP. The black arrows indicate the most significant modifications in the protein cavity, caused by residue mutations between both proteins, CEP and RPTP.

hydrogen-bonding interaction due to the Ser144 to Ala144 substitution and the presence of a bulky side chain occupying the volume of the additional binding site interfere with the interactions between the enzyme and potential small-molecule inhibitors, and consequently eliminate the enzymatic inhibition caused by them.

### 3.3.4. *Glycosylation pattern*

After the isolation and purification of the CEP from leaves of *C. excelsa* (in its native form), the SDS-PAGE analysis revealed a major protein band migrating at about 50 kDa. Since the theoretical molecular weight of the enzyme is 45 kDa, the higher experimentally observed molecular weight indicates that the enzyme has been glycosylated [3,30]. The presence of glycosylation sites was confirmed by high-resolution protein structure determination. The electron-density map clearly showed that CEP has five N-linked glycans at the positions of Asn8, Asn127, Asn185, Asn267 and Asn298, pointing away from the protein surface (Fig. 6A).

It has been reported that glycosylation increases the solubility of peroxidase in water solutions and improves peroxidase stability against proteolysis [59], but the details of how the glycosylation pattern influences the conformation and activity of peroxidases are largely unknown.

Here we compared the glycosylation pattern of the CEP and RPTP molecules (Fig. 6B). Although most of attached glycan chains were found in the same conserved positions, the degree of glycosylation varies, revealing a different number, and sometimes type, of inserted glycosides (Fig. 6C). For example, one of the longest glycan chains found in the CEP crystal structure was determined to be GlcNAc-GlcNA-Man, covalently attached to Asn298, while RPTP, at the same residue, displayed even longer chain comprising Man-[Man]Man-GlcNAc-[Fuc]GlcNAc (Fig. 6D). Not only does RPTP have

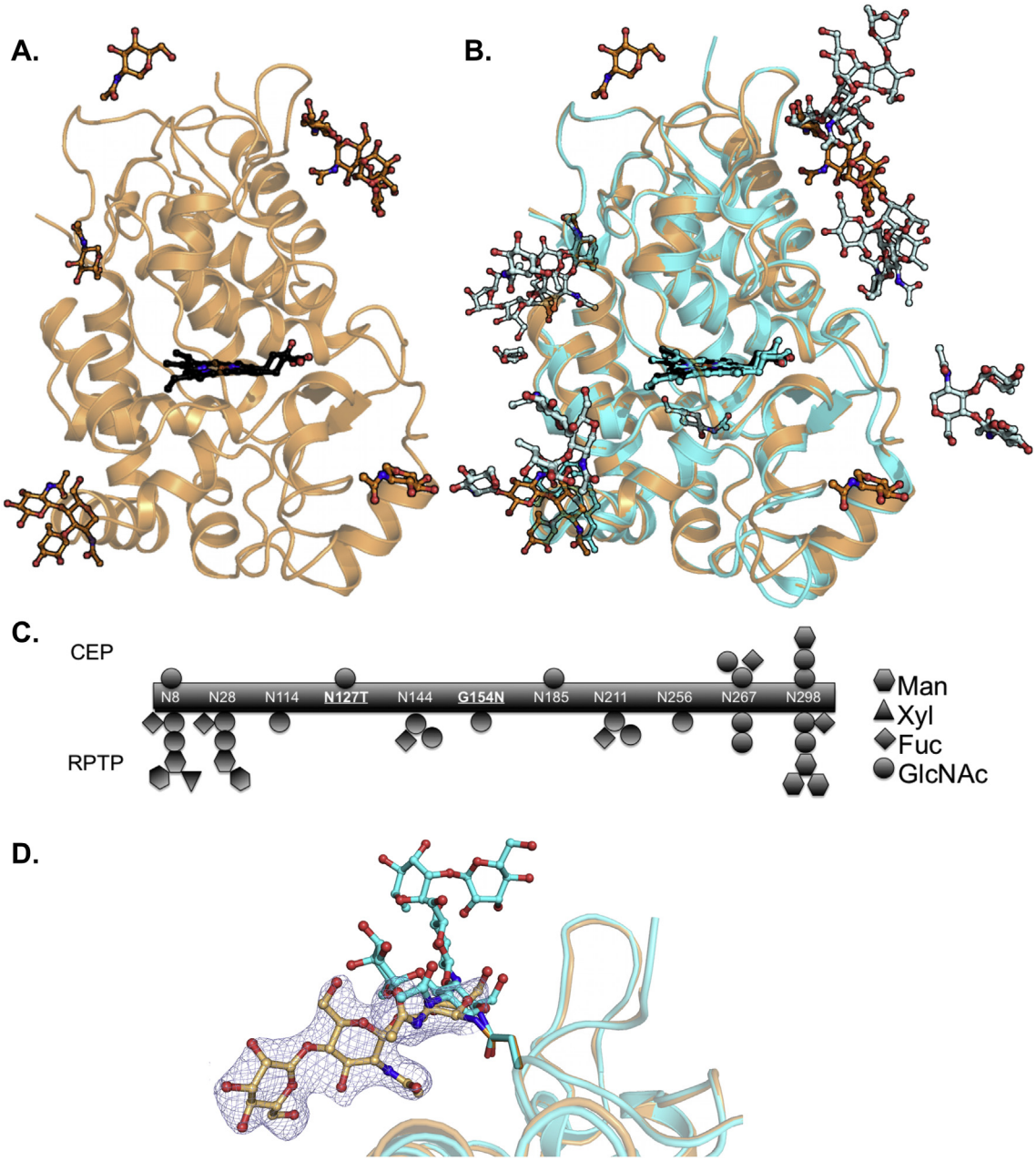


**Fig. 6.** Schematic representation of N-linked glycan chains found in the native CEP protein. A. X-ray structure of CEP showing the glycan chains attached to five asparagine residues and B. Comparison to the RPTP structure and its glycosylation. The sugar residues covalently attached to the protein chains are shown in stick representation. C. Schematic drawing of the glycosylation pattern of CEP (top) and RPTP (bottom). D. Detailed view of the CEP and RPTP protein surface around N298. The electron-density map ($2F_o - F_c$) contoured at 1.0σ shows the oligosaccharide GlcNAc-GlcNAc-Man attached to CEP (orange) and the oligosaccharide Man-Man-[Xyl]Man-GlcNAc-[Fuc]GlcNAc attached to RPTP.

a greater number of N-glycosylation sites decorated with longer glycan chains compared to CEP, but it also displays additional sites of N-glycosylation that are not found in CEP (Fig. 6). Both CEP (five N-glycosylation sites) and RPTP (nine N-glycosylation sites) are heavily glycosylated enzymes, which is consistent with the carbohydrate content found for other plant peroxidases studied, such as HRP-C, SBP and PNP, which display seven, five and three glycan chains, respectively [59].

Even considering the inherent difficulties involved in the comparison of glycosylation patterns, CEP and RPTP appear to have more glycan chains attached to the protein structure than some other homologous peroxidases. The heavy glycosylation of CEP might be important for protecting the enzyme from inactivation and ensuring its activity and stability [60,61].

### 3.4. Peroxidase dimerization

Previous biophysical experiments, including size-exclusion chromatography [19], DLS studies [30], analytical ultracentrifugation and high-sensitivity differential scanning calorimetry [10], have consistently demonstrated that both CEP and RPTP form dimers in solution. In order to investigate the molecular basis of their dimerization, we carried out a structural analysis of all possible

quaternary structures present in the CEP crystal and their potential molecular interfaces.

The homodimer observed in the asymmetric unit cell of the CEP crystal involves the formation of symmetric interfaces between two protein chains, where the contacts are arranged around the 2-fold NCS dimer axis. This dimer configuration was predicted to be the most feasible one by the PDBePISA package, an interactive tool for the investigation of macromolecular interfaces [62] revealing a large interface area of the molecular contact between the monomers (Fig. 7A). The interface area is approximately 780 $Å^2$ and comprises an interaction among 15 residues of each protein molecule: Ser197, Ser198, Ser199, Tyr200, Asp202, Leu203, Thr206, Lys207, Ser221, Ile224, Ile225, Pro227, Leu240, Thr241 and Leu242 (Fig. 7B). The majority of interactions is non-polar (42 non-bonded contacts), but also involve four hydrogen bonds between Ser197-Ile224 and Asp202-Lys207 (two hydrogen bonds from each pair of residues) (Fig. 7C). The surface of contact is quite distant from the active site and does not block the entrance to the heme-binding pocket.

In addition to the CEP dimer found in the asymmetric unit of the crystal, detailed analysis of the crystallographic symmetry allowed us to model another possible dimer configuration. This alternative configuration results in a much more modest interface, with an area of 291 $Å^2$ and 317 $Å^2$ for chains A and B, respectively. Consequently, fewer non-polar and polar interactions occur between chains.

Next, we compared these putative homodimers with all possible dimer arrangements existing in the crystal structure of the highly homologous enzyme, RPTP, which, as well as CEP, has also been implicated in dimer formation [10,30,48]. It is important to note that RPTP was crystallized in a different crystal form (space group $P3_12$) with a monomer of enzyme in the asymmetric unit and with completely different cell dimensions [15]. Remarkably, in spite of the different space groups of the CEP and RPTP crystals, the first dimer conformation of the CEP structure (dimer 1) described coincides with one of the homodimers of RPTP, identified through careful analysis of potential dimers generated by crystallographic symmetry operations of the corresponding crystal form. No other currently available plant peroxidase 3D structure presents either of the two putative dimeric assemblies of CEP.

The dimerization of CEP and RPTP has a direct influence on the mobility of the amino acid residues involved in the formation of the

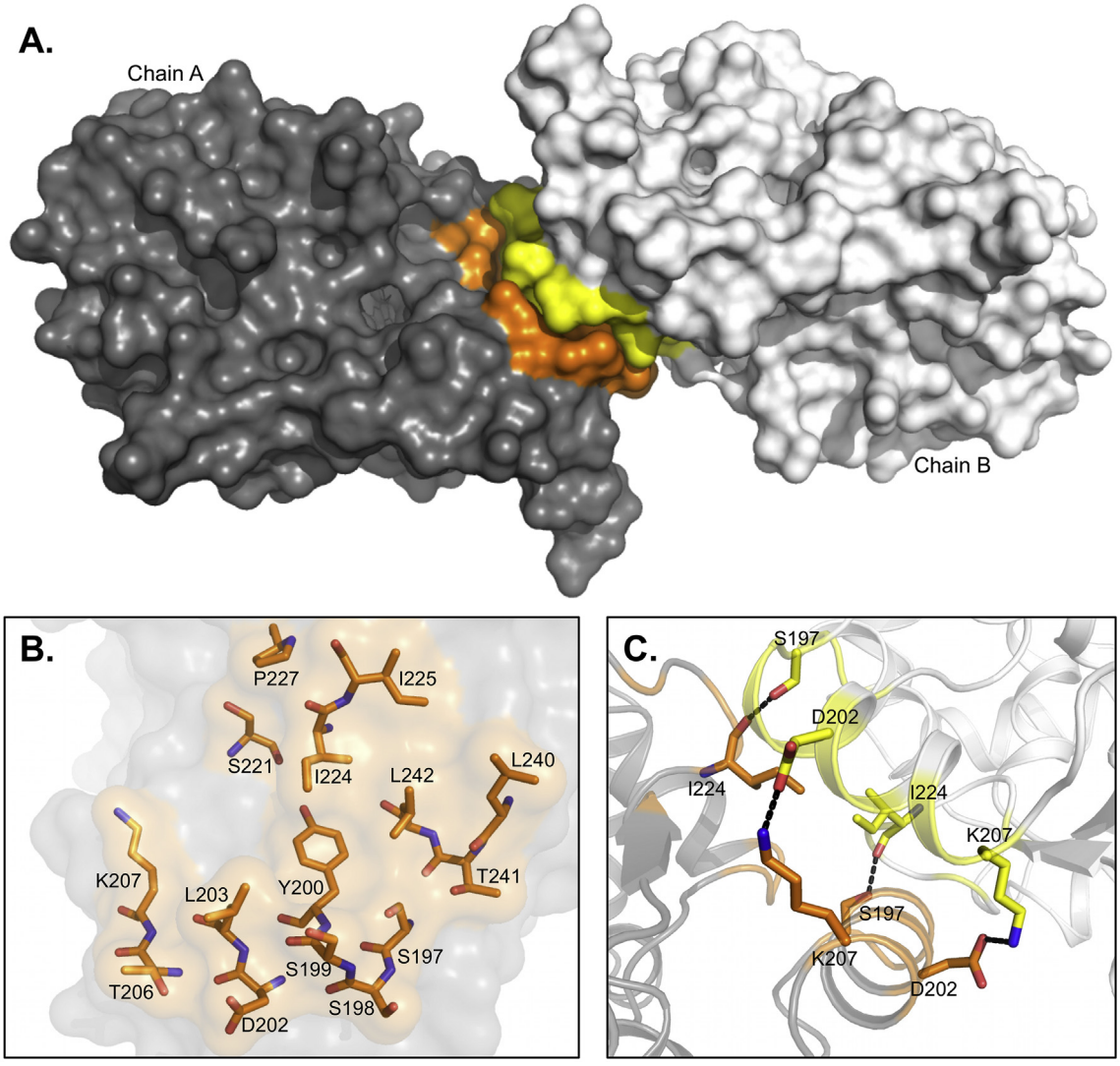


**Fig. 7.** CEP homodimer. A. Larger interface area of contact among the monomers (chain A and chain B interface are colored in orange and yellow, respectively). B. Residues involved in the interface interactions. C. Magnified stereo diagram of the CEP dimer 1 with the hydrogen bonds indicated by dashed lines.

dimer interface. The sequence alignment showed that all the residues involved in the interface (Fig. 2 – orange square) are located in the most variable region of protein sequence, in the peptide segment between the F and H helices, mainly comprising residues of the F″ helix. Most of these residues are conserved between CEP and RPTP, but are highly divergent between CEP and other enzymes. The non-conservation of the interface residues, including those involved in H-bond formation, is probably the main reason why the other peroxidases do not assemble in similar dimeric quaternary structures.

To check how dimer formation could provide stabilization for the CEP crystal, we performed an analysis of the B-factors of the peroxidase structures, which reflects the mobility, flexibility and conformational disorder of the enzymes. Consistently, the most variable region in the sequence alignment also showed the highest B-factors for all protein structures, except for the CEP and RPTP (Fig. 8A). This difference in mobility is clearly due to the dimerization interface, which decreases the mobility of residues 190 to 240 in both CEP and RPTP structures (Fig. 8B). We infer that the reduced dynamics and conformational flexibility of the residues at the dimerization interface would account for the stabilization of the CEP structure stabilization, previously identified in enzymatic studies of the peroxidases [38,48].

Although most previous works have proposed that native glycosylated peroxidases would not be able to form dimeric structures [7,8], and that only recombinant and non-glycosylated enzymes would tend to dimerize, our structural analysis for the first time reveals the molecular details of the dimerization of the heavily glycosylated native palm tree peroxidases CEP and RPTP, which has been suggested to be one of the reasons for their improved stability and robustness [10,19].

The connection between the dimerization process and peroxidase activity and stability are still poorly understood. Earlier calorimetric studies of ascorbate peroxidase have shown that dimerization contributes substantially to protein structure stability [63]. Whereas previous studies addressing recombinant horseradish peroxidase have shown that dimeric and monomeric forms of the enzyme display differences in enzyme activity and altered

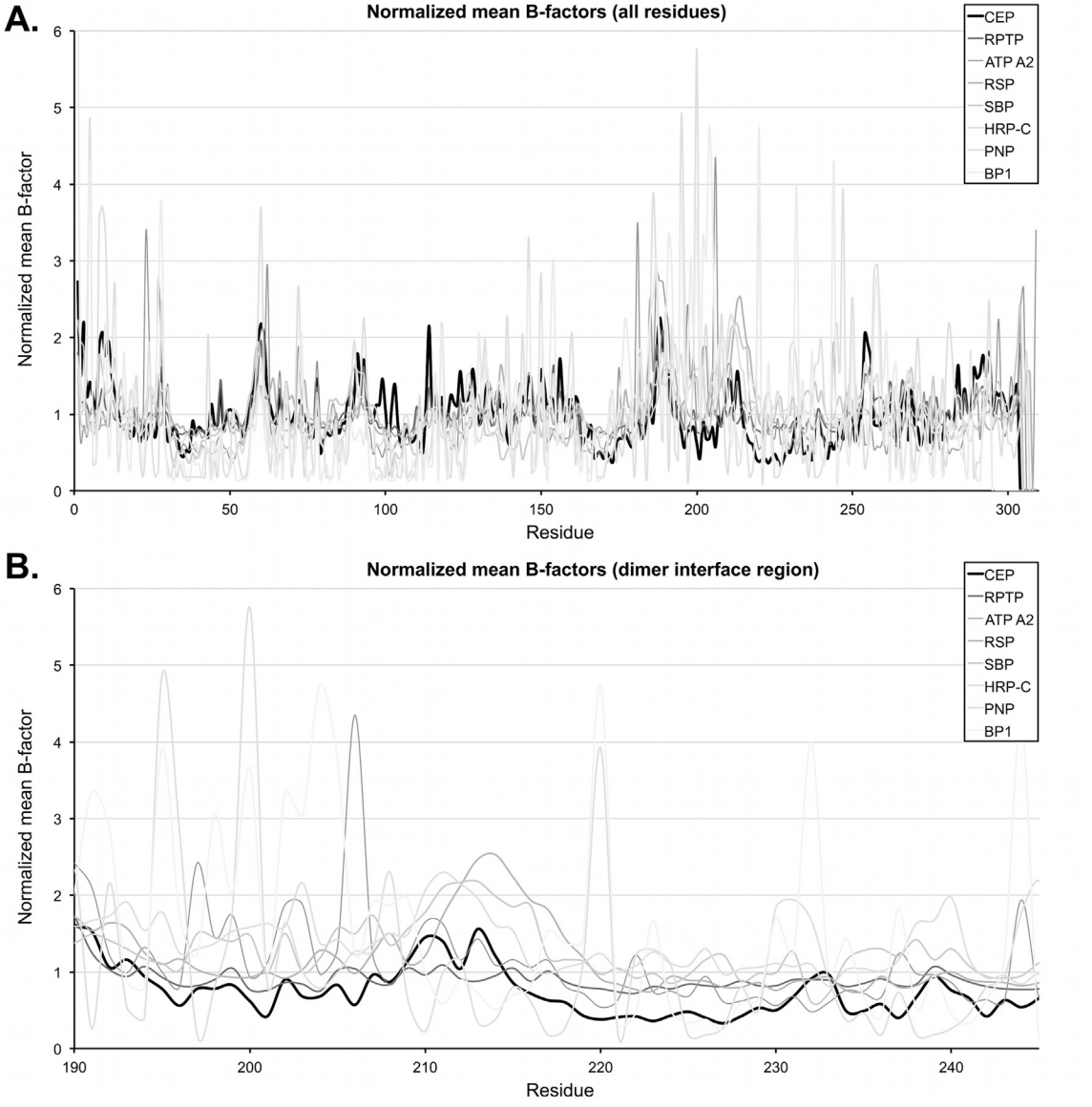


**Fig. 8.** Graphs of B-factor residues from the crystallographic structures. These graphs provide information about the conformational mobility of A. the entire structure and B. the residues that comprise the dimeric interface of CEP.

substrate specificity [7,53], this could be explained in terms of a restriction of the access of the substrate to the active site of the enzyme imposed by the dimeric form [9]. However, according to crystallographic models the possible dimeric structures of horseradish [9,25] and palm tree peroxidases have notable conformational differences. The dimer interface of CEP (and RPTP) does not overlap with the region of the active site and the substrate access channel. Thus, we advocate that the oligomerization of palm three peroxidases may promote a gain in the stability of the enzymes without compromising their catalytic activity.

## 4. Conclusions

Native peroxidase was successfully extracted and purified from the leaves of the palm tree *C. excelsa*, crystallized, and its structure was solved by protein crystallography. Consistent with other Class III peroxidases, the structure confirmed that CEP is N-glycosylated and revealed that CEP has a typical peroxidase fold.

Detailed structural analysis revealed a possible dimeric assembly, conserved amongst the plant palm peroxidases CEP and PRPT but absent in other known peroxidase structures. Such homodimer would account for the reduced mobility of the highly variable region between the H and F helices and might explain the improved stability of the latter enzymes.

Comparative analyses of the high-resolution X-ray structures of CEP and RPTP revealed important differences in the morphology of the opening of the active site, guaranteeing substrates' access to the heme group. The size and form of the entrance is related to the protection of the enzyme from inactivation by substrate radicals generated at the heme pocket and to the inhibition of the enzyme by small-molecule ligands (*e.g.*, buffer molecules).

## Conflict of interest

The authors declare that they have no competing interests.

## Acknowledgments

We are thankful to the Brazilian National Synchrotron Light Source (LNLS) and to the staff members of the MX2 beamline. This work was supported by Fundação de Amparo à Pesquisa do Estado de São Paulo (FAPESP) via research grants 2009/05349-6, 2008/56255-9, 2010/52362-5 and 2012/22802-9 and by Conselho Nacional de Desenvolvimento Científico e Tecnológico (CNPq) via grants # 490022/2009-0 and 373143/2012-5.

## Appendix A. Supplementary data

Supplementary data related to this article can be found at http://dx.doi.org/10.1016/j.biochi.2015.01.014.

## References

[1] T.L. Poulos, Peroxidases, Curr. Opin. Biotechnol. 4 (1993) 484–489.
[2] A.R. Barceló, R. Muñoz, Peroxidases: their role in the control of plant cell growth, in: C. Penel, T. Gaspar, H. Greppin (Eds.), Plant Peroxidases 1980–1990 Topics and Detailed Literature on Molecular, Biochemical, and Physiological Aspects, pp. 71–89.
[3] K.G. Welinder, J.M. Mauro, L. Nørskov-Lauritsen, Structure of plant and fungal peroxidases, Biochem. Soc. Trans. 20 (1992) 337–340.
[4] G. Smulevich, C. Jakopitsch, E. Droghetti, C. Obinger, Probing the structure and bifunctionality of catalase-peroxidase (KatG), J. Inorg. Biochem. 100 (2006) 568–585.
[5] S. Hiraga, K. Sasaki, H. Ito, Y. Ohashi, H. Matsui, A large family of class III plant peroxidases, Plant Cell Physiol. 42 (2001) 462–468.
[6] L. Almagro, L.V. Gómez Ros, S. Belchi-Navarro, R. Bru, A. Ros Barceló, M.A. Pedreño, Class III peroxidases in plant defence reactions, J. Exp. Bot. 60 (2009) 377–390.
[7] I.G. Gazaryan, N.L. Klyachko, Y.K. Dulkis, I.V. Ouporov, A.V. Levashov, Formation and properties of dimeric recombinant horseradish peroxidase in a system of reversed micelles, Biochem. J. 328 (1997) 643–647.
[8] W.R. Patterson, T.L. Poulos, Crystal structure of recombinant pea cytosolic ascorbate peroxidase, Biochemistry 34 (1995) 4331–4341.
[9] O.V. Ignatenko, A. Sjölander, D.M. Hushpulian, S.V. Kazakov, I.V. Ouporov, T.A. Chubar, A.A. Poloznikov, T. Ruzgas, V.I. Tishkov, L. Gorton, N.L. Klyachko, I.G. Gazaryan, Electrochemistry of chemically trapped dimeric and monomeric recombinant horseradish peroxidase, Adv. Biosens. Bioelectron. 2 (2013) 25–34.
[10] L.S. Zamorano, D.G. Pina, J.B. Arellano, S.A. Bursakov, A.P. Zhadan, J.J. Calvete, L. Sanz, P.R. Nielsen, E. Villar, O. Gavel, M.G. Roig, L. Watanabe, I. Polikarpov, V.L. Shnyrov, Thermodynamic characterization of the palm tree *Roystonea regia* peroxidase stability, Biochimie 90 (2008) 1737–1749.
[11] IYu Sakharov, Palm tree peroxidases, Biochemistry (Moscow) 69 (2004) 823–829.
[12] G.A. Petsko, Structural basis of thermostability in hyperthermophilic proteins, or "there's more than one way to skin a cat", Methods Enzymol. 334 (2001) 469–478.
[13] L. Banci, Structural properties of peroxidases, J. Biotechnol. 53 (1997) 253–263.
[14] C. Wang, M. Eufemi, C. Turano, A. Giartosio, Influence of the carbohydrate moiety on the stability of glycoproteins, Biochemistry 35 (1996) 7299–7307.
[15] L. Watanabe, P.R. de Moura, L. Bleicher, A.S. Nascimento, L.S. Zamorano, J.J. Calvete, L. Sanz, A. Pérez, S. Bursakov, M.G. Roig, V.L. Shnyrov, I. Polikarpov, Crystal structure and statistical coupling analysis of highly glycosylated peroxidase from royal palm tree (*Roystonea regia*), J. Struct. Biol. 169 (2010) 226–242.
[16] IYu Sakharov, J. Castillo, J.C. Areza, IYu Galaev, Purification and stability of peroxidase of African oil palm *Elaies guineensis*, Bioseparation 9 (2000) 125–132.
[17] I.Y. Sakharov, Long-term chemiluminescent signal is produced in the course of luminol peroxidation catalyzed by peroxidase isolated from leaves of African oil palm tree, Biochemistry (Moscow) 66 (2001) 515–519.
[18] A.V. Caramyshev, Y.N. Firsova, E.A. Slastya, A.A. Tagaev, N.V. Potapenko, E.S. Lobakova, O.Y. Pletjushkina, I.Y. Sakharov, Purification and characterization of windmill palm tree (*Trachycarpus fortunei*) peroxidase, J. Agric. Food Chem. 54 (2006) 9888–9894.
[19] L.S. Zamorano, S.B. Vilarmau, J.B. Arellano, G.G. Zhadan, N.H. Cuadrado, S.A. Bursakov, M.G. Roig, V.L. Shnyrov, Thermal stability of peroxidase from *Chamaerops excelsa* palm tree at pH 3, Int. J. Biol. Macromol. 44 (2009) 326–332.
[20] J.K. Kamal, M. Nazeerunnisa, D.V. Behere, A.K. Kizhakkedathu, Thermal unfolding of soybean peroxidase. Appropriate high denaturant concentrations induce cooperativity allowing the correct measurement of thermodynamic parameters, J. Biol. Chem. 277 (2002) 40717–40721.
[21] I.S. Alpeeva, M. Niculescu-Nistor, J.C. Leon, E. Csöregi, I.Y. Sakharov, Palm tree peroxidase-based biosensor with unique characteristics for hydrogen peroxide monitoring, Biosens. Bioelectron. 21 (2005) 742–748.
[22] G. Kenausis, Q. Chen, A. Heller, Electrochemical glucose and lactate sensors based on "wired" thermostable soybean peroxidase operating continuously and stably at 37 degrees C, Anal. Chem. 69 (1997) 1054–1060.
[23] B. Wang, B. Li, Z. Wang, G. Xu, Q. Wang, S. Dong, Sol-gel thin-film immobilized soybean peroxidase biosensor for the amperometric determination of hydrogen peroxide in acid medium, Anal. Chem. 71 (1999) 1935–1939.
[24] A.M. Azevedo, V.C. Martins, D.M. Prazeres, V. Vojinović, J.M. Cabral, L.P. Fonseca, Horseradish peroxidase: a valuable tool in biotechnology, Biotechnol. Annu. Rev. 9 (2003) 199–247.
[25] M. Gajhede, D.J. Schuller, A. Henriksen, A.T. Smith, T.L. Poulos, Crystal structure of horseradish peroxidase C at 2.15 A resolution, Nat. Struct. Biol. 4 (1997) 1032–1038.
[26] D.J. Schuller, N. Ban, R.B. Huystee, A. McPherson, T.L. Poulos, The crystal structure of peanut peroxidase, Structure 4 (1996) 311–321.
[27] A. Henriksen, K.G. Welinder, M. Gajhede, Structure of barley grain peroxidase refined at 1.9-A resolution. A plant peroxidase reversibly inactivated at neutral pH, J. Biol. Chem. 273 (1998) 2241–2248.
[28] L. Ostergaard, K. Teilum, O. Mirza, O. Mattsson, M. Petersen, K.G. Welinder, J. Mundy, M. Gajhede, A. Henriksen, Arabidopsis ATP A2 peroxidase. Expression and high-resolution structure of a plant peroxidase with implications for lignification, Plant Mol. Biol. 44 (2000) 231–243.
[29] A. Henriksen, O. Mirza, C. Indiani, K. Teilum, G. Smulevich, K.G. Welinder, M. Gajhede, Structure of soybean seed coat peroxidase: a plant peroxidase with unusual stability and haem-apoprotein interactions, Protein Sci. 10 (2001) 108–115.
[30] L.C. Textor, J.C. Santos, N.H. Cuadrado, M.G. Roig, G.G. Zhadan, V.L. Shnyrov, I. Polikarpov, Purification, crystallization and preliminary crystallographic analysis of peroxidase from the palm tree *Chamaerops excelsa*, Acta Crystallogr. Sect. F Struct. Biol. Cryst. Commun. 67 (2011) 1641–1644.
[31] B.G. Guimaraes, L. Sanfelici, R.T. Neuenschwander, F. Rodrigues, W.C. Grizolli, M.A. Raulik, J.R. Piton, B.C. Meyer, A.S. Nascimento, I. Polikarpov, The MX2 macromolecular crystallography beamline: a wiggler X-ray source at the LNLS, J. Synchrotron Radiat. 16 (2009) 69–75.
[32] W. Kabsch, XDS, Acta Crystallogr. D Biol. Crystallogr. 66 (2010) 125–132.
[33] A.J. McCoy, R.W. Grosse-Kunstleve, P.D. Adams, M.D. Winn, L.C. Storoni, R.J. Read, Phaser crystallographic software, J. Appl. Crystallogr. 40 (2007) 658–674.

[34] P. Emsley, B. Lohkamp, W.G. Scott, K. Cowtan, Features and development of Coot, Acta Crystallogr. D Biol. Crystallogr. 66 (2010) 486–501.
[35] G.N. Murshudov, P. Skubák, A.A. Lebedev, N.S. Pannu, R.A. Steiner, R.A. Nicholls, M.D. Winn, F. Long, A.A. Vagin, REFMAC5 for the refinement of macromolecular crystal structures, Acta Crystallogr. D Biol. Crystallogr. 67 (2011) 355–367.
[36] S.X. Cohen, M. Ben Jelloul, F. Long, A. Vagin, P. Knipscheer, J. Lebbink, T.K. Sixma, V.S. Lamzin, G.N. Murshudov, A. Perrakis, ARP/wARP and molecular replacement: the next generation, Acta Crystallogr. D Biol. Crystallogr. 64 (2008) 49–60.
[37] V.B. Chen, W.B. Arendall, J.J. Headd, D.A. Keedy, R.M. Immormino, G.J. Kapral, L.W. Murray, J.S. Richardson, D.C. Richardson, MolProbity: all-atom structure validation for macromolecular crystallography, Acta Crystallogr. D Biol. Crystallogr. 66 (2010) 12–21.
[38] N.H. Cuadrado, G.G. Zhadan, M.G. Roig, V.L. Shnyrov, Suicide inactivation of peroxidase from *Chamaerops excelsa* palm tree leaves, Int. J. Biol. Macromol. 49 (2011) 1078–1082.
[39] G.S. Zakharova, I.V. Uporov, V.I. Tishkov, Horseradish peroxidase: modulation of properties by chemical modification of protein and heme, Biochemistry (Moscow) 76 (2011) 1391–1401.
[40] M. Laberge, T. Yonetani, J. Fidy, Normal coordinate structural decomposition of the heme distortions of hemoglobin in various quaternary states and bound to allosteric effectors, Mol. Divers. 7 (2003) 15–23.
[41] K. Szigeti, L. Smeller, S. Osváth, Z. Majer, J. Fidy, The structure of horseradish peroxidase C characterized as a molten globule state after Ca(2+) depletion, Biochim. Biophys. Acta 1784 (2008) 1965–1974.
[42] L.M. Lagrimini, W. Burkhart, M. Moyer, S. Rothstein, Molecular cloning of complementary DNA encoding the lignin-forming peroxidase from tobacco: molecular analysis and tissue-specific expression, Proc. Natl. Acad. Sci. U. S. A. 84 (1987) 7542–7546.
[43] M.G. Murray, L.M. Hoffman, N.P. Jarvis, Improved yield of full-length phaseolin cDNA clones by controlling premature anticomplementary DNA synthesis, Plant Mol. Biol. 2 (1983) 75–83.
[44] C. Penel, T. Caspar, H. Greppin, Plant Peroxidases, 1980–1990.
[45] T.L. Poulos, J. Kraut, The stereochemistry of peroxidase catalysis, J. Biol. Chem. 255 (1980) 8199–8205.
[46] C.B. Rasmussen, H.B. Dunford, K.G. Welinder, Rate enhancement of compound I formation of barley peroxidase by ferulic acid, caffeic acid, and coniferyl alcohol, Biochemistry 34 (1995) 4022–4029.
[47] L.S. Zamorano, N.H. Cuadrado, P.P. Galende, M.G. Roig, Steady-state kinetics of *Roystonea regia* palm tree peroxidase, J. Biophys. Chem. 3 (2012) 16–28.
[48] N.H. Cuadrado, J.B. Arellano, J.J. Calvete, L. Sanz, G.G. Zhadan, I. Polikarpov, S. Bursakov, M.G. Roig, V.L. Shnyrov, Substrate specificity of the *Chamaerops excelsa* palm tree peroxidase. A steady-state kinetic study, J. Mol. Catal. B Enzym. 74 (2012) 103–108.
[49] R. Nakajima, I. Yamazaki, The mechanism of oxyperoxidase formation from ferryl peroxidase and hydrogen peroxide, J. Biol. Chem. 262 (1987) 2576–2581.
[50] M.B. Arnao, M. Acosta, J.A. del Río, F. García-Cánovas, Inactivation of peroxidase by hydrogen peroxide and its protection by a reductant agent, Biochim. Biophys. Acta 1038 (1990) 85–89.
[51] J. Wilce, J. Vivian, M. Wilce, Oligonucleotide binding proteins: the occurrence of dimer and multimer formation, Adv. Exp. Med. Biol. 747 (2012) 91–104.
[52] M. Gajhede, Plant peroxidases: substrate complexes with mechanistic implications, Biochem. Soc. Trans. 29 (2001) 91–98.
[53] N.C. Veitch, Horseradish peroxidase: a modern view of a classic enzyme, Phytochemistry 65 (2004) 249–259.
[54] T.L. Poulos, Heme enzyme structure and function, Chem. Rev. 114 (2014) 3919–3962.
[55] D. Nonaka, H. Wariishi, H. Fujii, Paramagnetic 13C and 15N NMR analyses of cyanide- (13C15N-) ligated ferric peroxidases: the push effect, not pull effect, modulates the compound I formation rate, Biochemistry 48 (2009) 898–905.
[56] A. Hörlein, A. Näär, T. Heinzel, J. Torchia, B. Gloss, R. Kurokawa, A. Ryan, Y. Kamei, M. Söderström, C. Glass, Ligand-independent repression by the thyroid hormone receptor mediated by a nuclear receptor co-repressor, Nature 377 (1995) 397–404.
[57] B.J. Ryan, N. Carolan, C. O'Fágáin, Horseradish and soybean peroxidases: comparable tools for alternative niches? Trends Biotechnol. 24 (2006) 355–363.
[58] A. Henriksen, A.T. Smith, M. Gajhede, The structures of the horseradish peroxidase C-ferulic acid complex and the ternary complex with cyanide suggest how peroxidases oxidize small phenolic substrates, J. Biol. Chem. 274 (1999) 35005–35011.
[59] R.B. van Huystee, M.G. Roig, V.L. Shnyrov, I.Y. Sakharov, Peroxidase stability related to its calcium and glycans, Phytochem. Rev. 3 (2004) 19–28.
[60] M.R. Wormald, R.A. Dwek, Glycoproteins: glycan presentation and protein-fold stability, Structure 7 (1999) R155–R160.
[61] S.R. Hanson, E.K. Culyba, T.L. Hsu, C.H. Wong, J.W. Kelly, E.T. Powers, The core trisaccharide of an N-linked glycoprotein intrinsically accelerates folding and enhances stability, Proc. Natl. Acad. Sci. U. S. A. 106 (2009) 3131–3136.
[62] E. Krissinel, K. Henrick, Inference of macromolecular assemblies from crystalline state, J. Mol. Biol. 372 (2007) 774–797.
[63] D. Mandelman, F.P. Schwarz, H. Li, T.L. Poulos, The role of quaternary interactions on the stability and activity of ascorbate peroxidase, Protein Sci. 7 (1998) 2089–2098.